The Effect of Cloud Type on Earth's Energy Balance: Global Analysis

DENNIS L. HARTMANN, MAUREEN E. OCKERT-BELL, AND MARC L. MICHELSEN

Department of Atmospheric Sciences, University of Washington, Seattle, Washington

(Manuscript received 10 September 1991, in final form 10 February 1992)

ABSTRACT

The role of fractional area coverage by cloud types in the energy balance of the earth is investigated through joint use of International Satellite Cloud Climatology Project (ISCCP) C1 cloud data and Earth Radiation Budget Experiment (ERBE) broadband energy flux data for the one-year period March 1985 through February 1986. Multiple linear regression is used to relate the radiation budget data to the cloud data. Comparing cloud forcing estimates obtained from the ISCCP–ERBE regression with those derived from the ERBE scene identification shows generally good agreement except over snow, in tropical convective regions, and in regions that are either nearly cloudless or always overcast. It is suggested that a substantial fraction of the disagreement in longwave cloud forcing in tropical convective regions is associated with the fact that the ERBE scene identification does not take into account variations in upper-tropospheric water vapor. On a global average basis, low clouds make the largest contribution to the net energy balance of the earth, because they cover such a large area and because their albedo effect dominates their effect on emitted thermal radiation. High, optically thick clouds can also very effectively reduce the energy balance, however, because their very high albedos overcome their low emission temperatures.

1. Introduction

The effect of clouds on the energy balance of the earth and their role in climate sensitivity have been topics of intense interest in recent years (e.g., Schneider 1972; Cess 1976; Wetherald and Manabe 1980; Hansen et al. 1984; Hartmann et al. 1986), although the radiative effects of clouds have long been recognized as a critical component of climate (Abbott and Fowle 1908; Haurwitz 1948). The goal of many of the early papers was to examine the change in net radiation at the top of the atmosphere caused by a change in total cloud cover. Such analyses ignore the critical role of cloud optical properties and cloud-top temperature in determining net radiation, and fail to make a connection between the radiative effects of clouds and the mechanisms whereby the clouds are generated. Simultaneous estimates of cloud distributions and top-of-atmosphere radiative fluxes make it possible to study the effect of individual cloud types on the energy balance of the earth.

In a previous paper, Ockert-Bell and Hartmann (1992, hereafter referred to as OBH) investigated the relationship between the radiative energy balance at the top of the atmosphere measured by the Earth Radiation Budget Experiment (ERBE) and the cloud field measured by the International Satellite Cloud Climatology Project (ISCCP). In OBH the usefulness of linear techniques for revealing relationships between cloud amount and radiation budget quantities was investigated for six regions that characterize tropical convective, stratus, and midlatitude synoptic cloud regimes. It was shown that the 35 ISCCP cloud types can be simplified into five cloud types, which will explain as much of the variance of the ERBE radiation budget parameters as any other combination of ISCCP cloud types. For daily mean data in 2.5° × 2.5° regions the ISCCP estimates of the fractional coverage of five cloud types explain more than 80 percent of the variance of OLR and albedo in most of the regions investigated by OBH. Net radiation, on the other hand, was rather poorly predicted by ISCCP cloud information, with only about 40 to 60 percent of the variance predicted in typical cases. It was also shown that cloud-type information is critical to the radiation balance, since regressions on total cloud cover alone predicted a much smaller fraction of the variance than the five-type description of clouds. These results are in general agreement with the conclusions of Dhuria and Kyle (1991), who performed a similar analysis using cloud and radiation budget data from the *Nimbus-7* satellite. The goal of the present paper is to extend this type of analysis to the globe, and to present the results in map form, so that the geographical structure of cloud type and its effect on the radiation balance will be apparent. Global averages will also be presented.

A multiple linear regression procedure is used to express ERBE radiation budget quantities as functions of the fractional area coverage by five generic types of

Corresponding author address: Prof. Dennis L. Hartmann, Department of Atmospheric Sciences, AK-40, University of Washington, Seattle, WA 98195.

cloud. For guidance in assessing the usefulness of this technique we consider the fraction of explained variance achieved by the regression, and compare the cloud radiative forcing implied from the regression with the cloud radiative forcing provided by the ERBE clear-sky climatology. It is understood that the regression method will fail to properly represent the relationship between clouds and radiation balance quantities where the data do not adequately describe this relationship. The most serious problems will arise where a region is almost totally cloud covered during the period of observation, since in such cases the regression is not given any information about what the radiative energy fluxes are in the absence of clouds. The occurrence of a regression failure of this type can be adequately diagnosed, and does not preclude the use and interpretation of the regression results in regions where the data do adequately describe the relationships of interest. Where the regression estimates of cloud forcing agree with ERBE estimates, we regard the agreement as a form of validation for both estimates. The agreement between the cloud-type regressions and the ERBE climatology is good enough in most regions that we proceed to an interpretation of the importance of individual cloud types for the energy balance of the earth. For those regions and seasons where the ERBE cloud forcing and the results from this study differ significantly, we discuss possible reasons for the differences.

2. Data and technique

The ERBE data measure the broadband fluxes of solar and terrestrial radiation at the top of the atmosphere (Barkstrom and Smith 1986). The ISCCP C-1 dataset characterizes the cloud cover in terms of the area coverage by clouds with tops in seven pressure intervals and visible optical depths in five intervals, giving a total of 35 possible cloud types (Rossow and Schiffer 1991). In OBH it was argued that these 35 types can be reduced to five, as shown in Fig. 1, without much reduction in ability to define day-to-day variations in radiation budget quantities. The clouds can be divided into high, middle, and low, according to the pressure at cloud top, and into thin and thick according to the visible optical depth. As explained in OBH, we break the optical depth categories at an optical depth of 9.38, which is near the optical depth above which the albedo becomes insensitive to optical depth. We will refer to the category with optical depths less than 9.38 as the "thin" category, even though clouds with optical depths between 1 and 9 can hardly be regarded as optically thin by the usual definition. The low-cloud category is not divided into thin and thick, because it is not useful in the regression analysis to follow, primarily because most of the low cloud is of the thin variety. The simplification of the ISCCP cloud types illustrated in Fig. 1 has several virtues, as demonstrated in OBH. The first is simplicity. With five cloud types

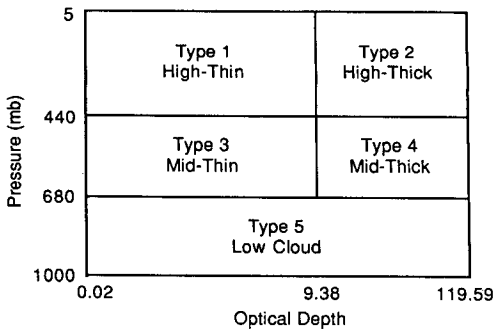

FIG. 1. Diagram showing the five cloud types used in this analysis.

it is possible to relatively easily describe a relationship between cloud type and radiation balance that is both intuitive and quantitative. More important, as shown in OBH, the five-cloud-type description is able to "explain" the day-to-day variations in radiation budget quantities as well as any other cloud description. This is not because the variations of cloud-top pressure and cloud optical depth within the five categories are not important, but rather because the amounts in adjacent categories tend to be correlated with each other.

Both the ERBE and ISCCP data are presented for 2.5° × 2.5° latitude–longitude regions, for which estimates of daily-mean values have been constructed. The data used here for regressions between ERBE and ISCCP data come from the single year beginning in March of 1985 and concluding in February of 1986. In OBH the regressions were performed on daily data for single months with six adjacent 2.5° regions grouped together and considered independent realizations. Here we use three-month seasons of daily data and perform the regressions separately for each individual 2.5° region, so that the geographical structure of the results is brought out. Three passes of a 1–2–1 smoother are applied to the results before plotting. We will focus primarily on the solstitial seasons of June through August 1985 (JJA) and December 1985 through February 1986 (DJF). The equinoctial seasons have been analyzed in the same way, and show very similar relationships.

The geographical distributions of high, low, and total cloud cover are shown in Figs. 2 and 3 for the solstitial seasons. Since we require a visible measurement to define the optical depth of cloud, the cloud data are unavailable where the insolation falls below the level necessary for measurement. Therefore, no data are available poleward of about 60° latitude in the winter hemisphere. The high-cloud types occur preferentially where convection occurs in the tropics and in midlatitude storm tracks. High thick clouds occur in a smaller fraction of the globe than high thin clouds and in those regions where the convection is the most active. Low clouds appear to be predominantly oceanic, and most abundant in the subtropical eastern oceans, where the

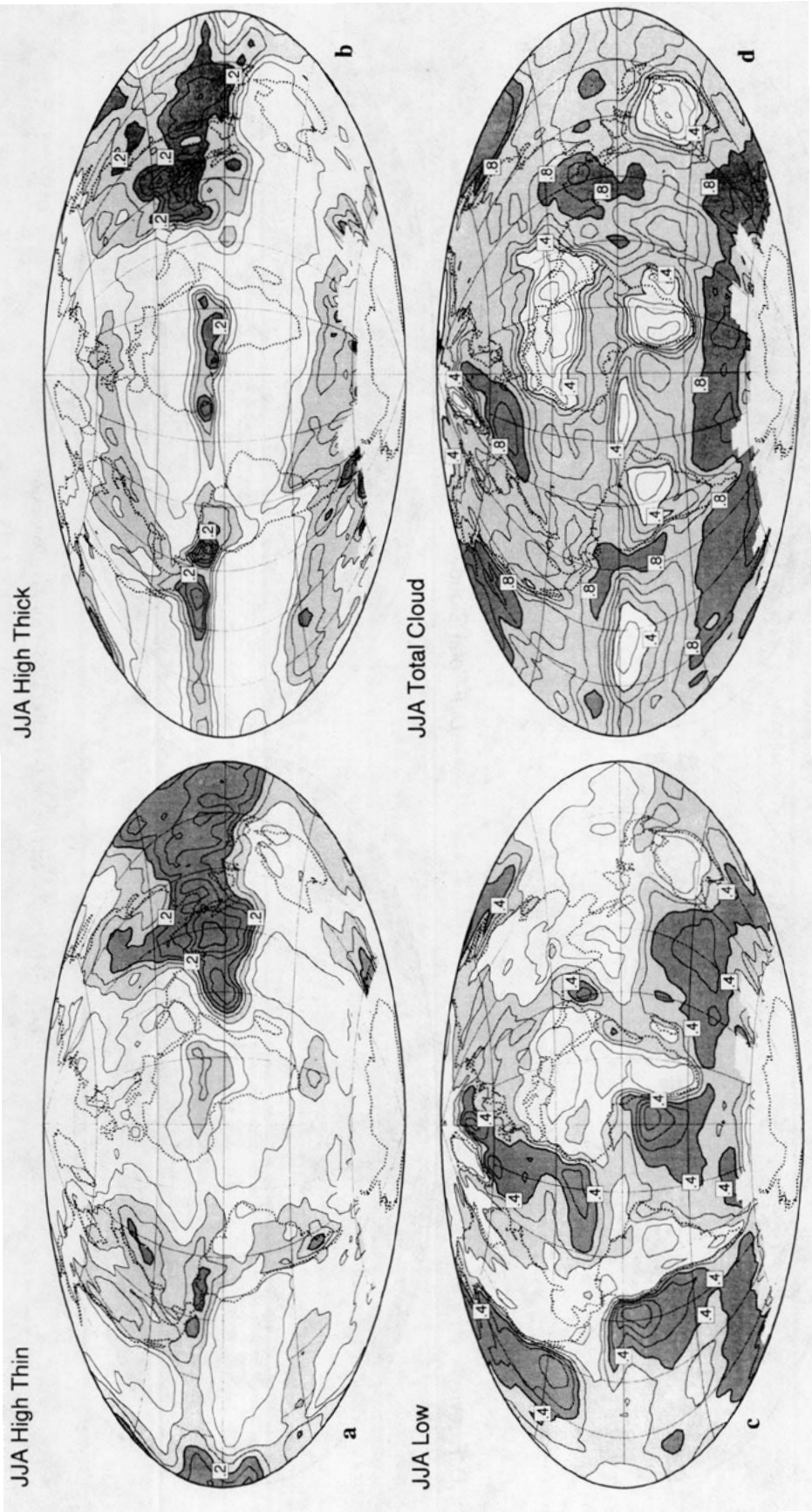

FIG. 2. Geographical distributions of cloud fractional coverage for some of the categories of cloud defined by Fig. 1 during the June–August 1986 season. (a) High thin cloud (contour interval 0.05, values greater than 0.1—light shading, values greater than 0.2—heavy shading), (b) high thick cloud, (c) low cloud (contour interval 0.1, shading changes at 0.2 and 0.4), (d) total cloud cover (contour interval 0.1, shading changes at 0.4 and 0.8). Missing values occur where the insolation is small.

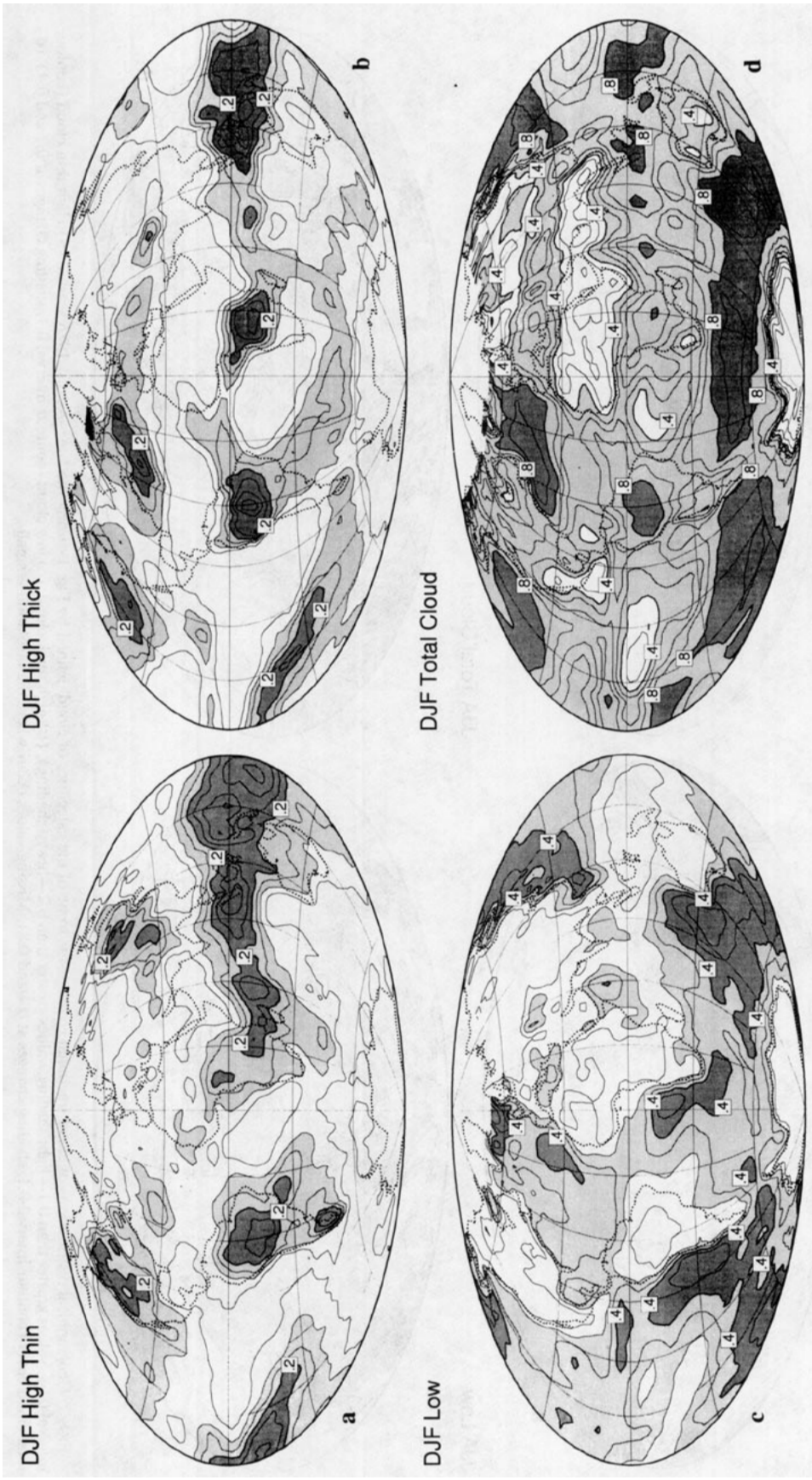

FIG. 3. As in Fig. 2 except for the December 1985–February 1986 season.

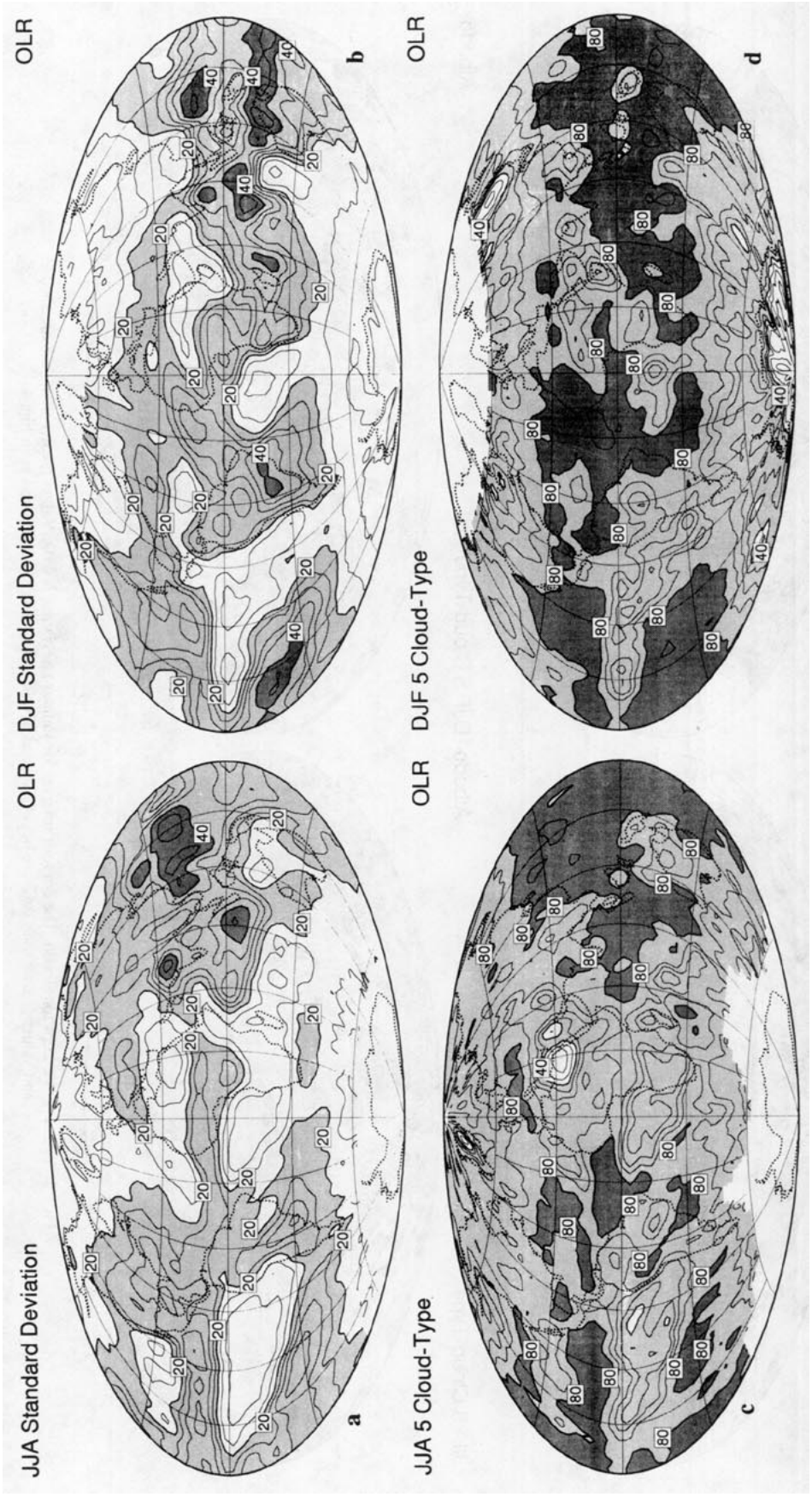

FIG. 4. Standard deviation of OLR and fraction of variance of OLR explained by the regression on five ISCCP cloud types for JJA and DJF seasons. Contour interval for standard deviation is 5 W m^{-2}. Values greater than 20 W m^{-2} are shaded and values greater than 40 W m^{-2} are heavily shaded. Contour interval for fraction of explained variance is 10%. Values greater than 40% are shaded and values greater than 80% are heavily shaded.

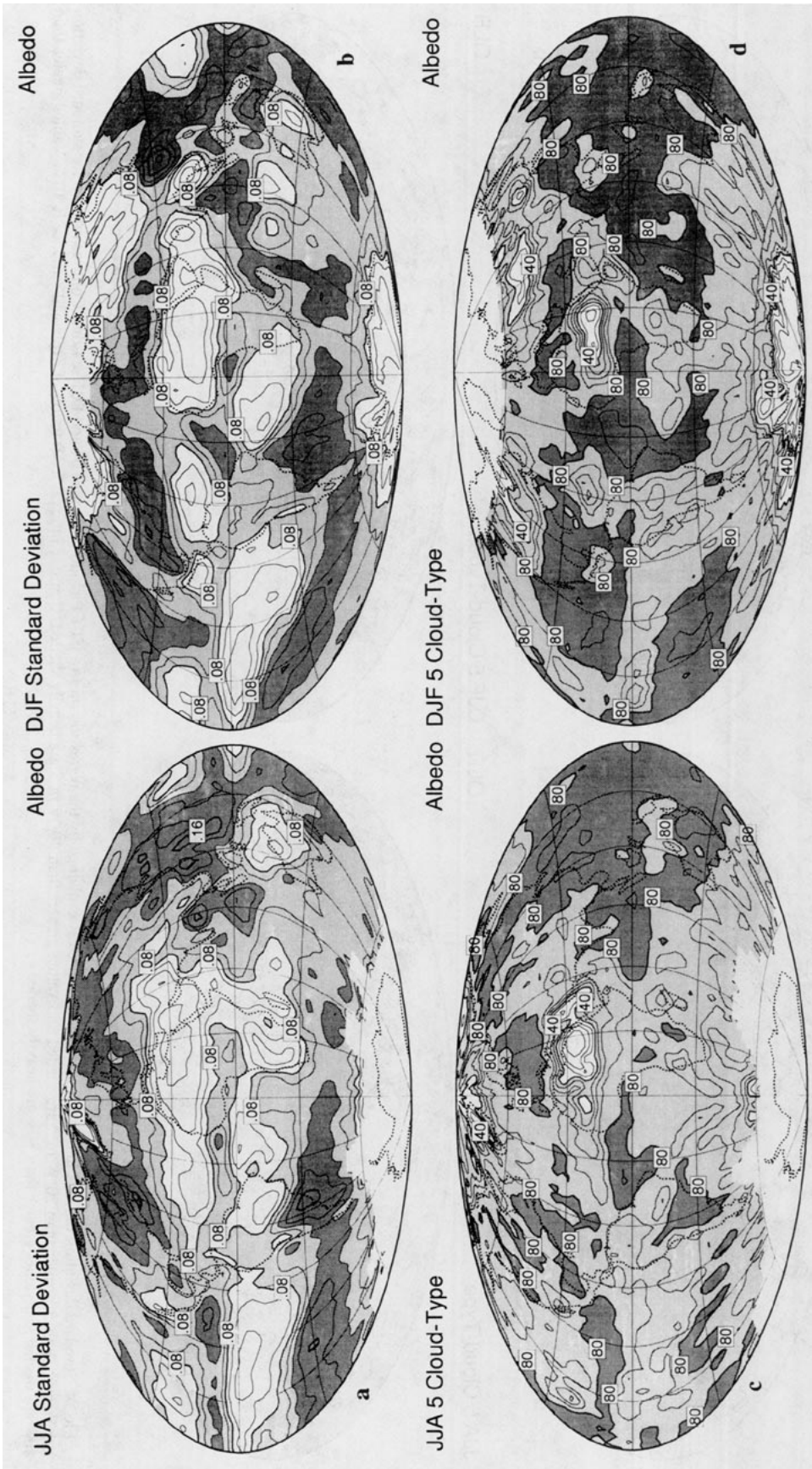

FIG. 5. As in Fig. 4 except for albedo. The contour interval for standard deviation is 0.02. Values greater than 0.08 are shaded and values greater than 0.12 are heavily shaded. Explained variance is contoured as in Fig. 4.

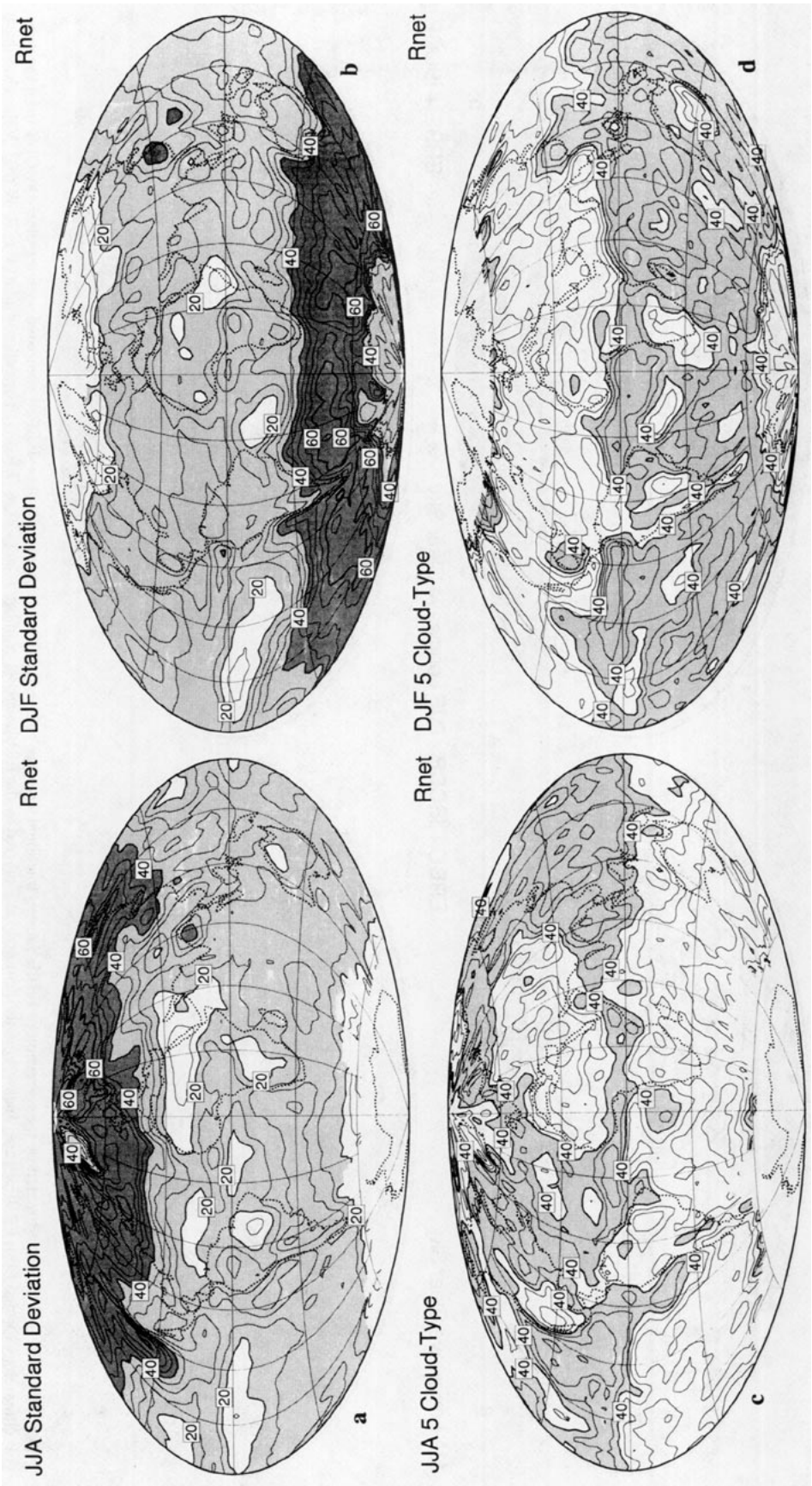

FIG. 6. As in Fig. 4 except for net radiation given in W m^{-2}.

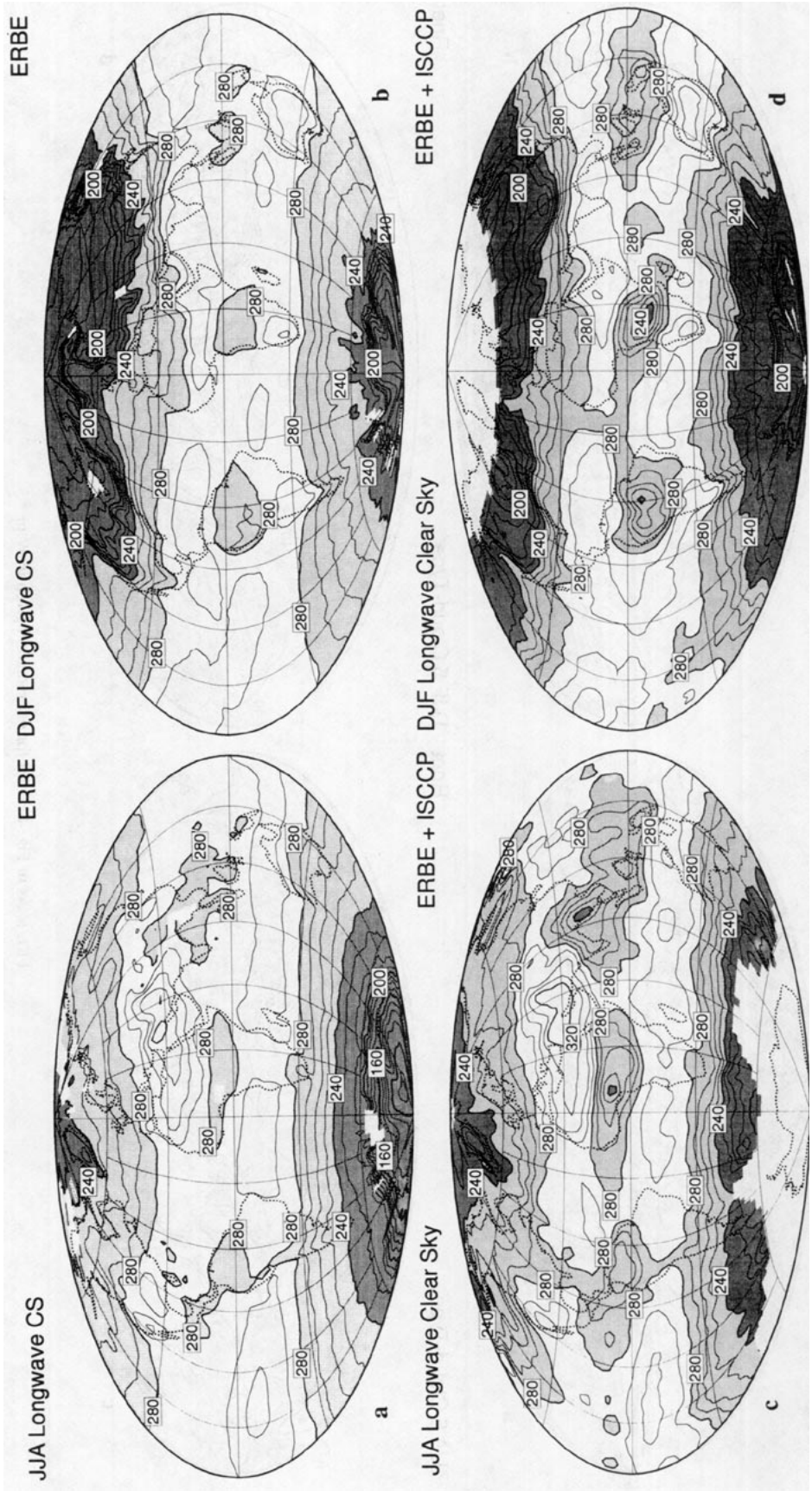

FIG. 7. The clear-sky OLR estimated by the regression of ERBE data on fractional coverage by five ISCCP cloud types (ERBE + ISCCP) compared with the clear-sky OLR from the two-year climatology formed from ERBE scanner measurements identified as cloud-free by the ERBE scene-identification algorithm (ERBE). The contour interval is 20 W m^{-2}. Values less than 280 are shaded and values less than 240 W m^{-2} are heavily shaded.

sea surface temperature is comparatively low and where the mean air motion is downward. Total cloud cover is greatest over the high-latitude oceans, where stratus regimes are best developed, and in regions of intense tropical convection, such as the Bay of Bengal during JJA and over the Amazon and Indonesia during DJF. The middle-level, thin clouds are distributed diffusely over the convective regions of the earth and their surroundings (not shown). Middle-level, thick clouds occur mostly in high latitudes (not shown).

3. Regression results

The relationship of ISCCP cloud amount data to ERBE radiation budget data has been measured by using stepwise multiple linear regression to express the radiation budget data in terms of cloud abundance (OBH). Regressions are performed to explain the day-to-day variation of 24-h means over three-month seasons for each 2.5° region over the globe where data are available.

a. Explained variance

Figures 4, 5, and 6 show the standard deviations of daily values of radiation budget quantities and the fraction of variance explained by the regression on the five cloud types. For OLR (Fig. 4) and albedo (Fig. 5) the regression explains 80 percent or more of the variance, in those regions where the variance is large. In regions where the cloud amount is small, or the effect of cloud on the quantity of interest is small, the standard deviation is small and the regression is of low quality. Such regions occur mostly in the tropics and arid regions where large-scale downward motion suppresses cloudiness. The fraction of variance explained by the five-cloud-type description of cloudiness is generally about double of that explained by regression on total cloud cover alone (not shown). The increase in explained variance associated with cloud-type information depends on the complexity of the cloud field. In regions where a single cloud type is dominant, such as stratus cloud regions without overlying cirrus, the total cloud cover does a good job of explaining the albedo and OLR variations associated with clouds. Where clouds have more variable optical properties and structure, as in tropical convective regions or midlatitude cyclone tracks, cloud-type changes are essential in determining the day-to-day variations of radiation budget quantities.

Some geographical features of the variance, explained variance, and cloud cover are interesting and will become important later. For example, consider the standard deviation of OLR in Indian Ocean regions during JJA (Fig. 4a). The standard deviation of OLR has maxima over northwest India and west of Sumatra. Between these two regions the standard deviation is less, and a pronounced minimum appears over the coastal areas of Pakistan and Burma. The total fractional area coverage of cloud exceeds 90 percent along the coast of Burma (Fig. 2d), where the fractional coverage of high, thick convective cloud is greatest (Fig. 2b). Even though clouds with high tops are abundant in this region, the variation of OLR is less than some other regions, because the convective clouds are so abundant and persistent. The albedo also has a relatively small standard deviation in this region (Fig. 5c). The regression procedure may have difficulty in properly defining the role of clouds on the energy balance in regions where clear skies are almost never observed, even if the regression may explain a large fraction of the variance. Another example of a region with cloudiness greater than 90 percent is the middle and high latitudes of the Southern Hemisphere and the oceanic storm tracks of the Northern Hemisphere.

The standard deviation of net radiation is strongly affected by the amount of insolation and the albedo of the clouds, which is in turn related to the solar zenith angle. The variation of net radiation is also dependent on the degree of cancellation between the effect of clouds on the albedo and the OLR. These two effects cancel more completely in the tropics. These factors cause the largest day-to-day variability in net radiation to occur in the high latitudes, especially those of the summer hemisphere (Figs. 6a and 6c). During the equinoctial seasons the variability of net radiation is more symmetrically distributed, with the largest values in the middle and high latitudes of both hemispheres (not shown).

ISCCP cloud amounts can explain a much smaller fraction of the variance of net radiation than of OLR or albedo (Fig. 6b and 6d). In the summer hemisphere, typically more than 40 percent of the variance of net radiation is explained by the data on cloud type, but in the winter hemisphere less than 40 percent is explained, except in stratus regions. The primary reason for the smaller fraction of explained variance of net

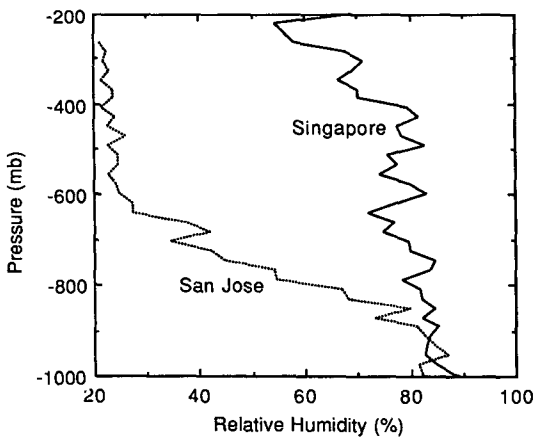

FIG. 8. Relative humidity profiles from Singapore, Indonesia, averaged for Oct–Dec 1985 (solid) and San Jose, Puerto Rico, averaged for December 1985 through February 1986 (dashed).

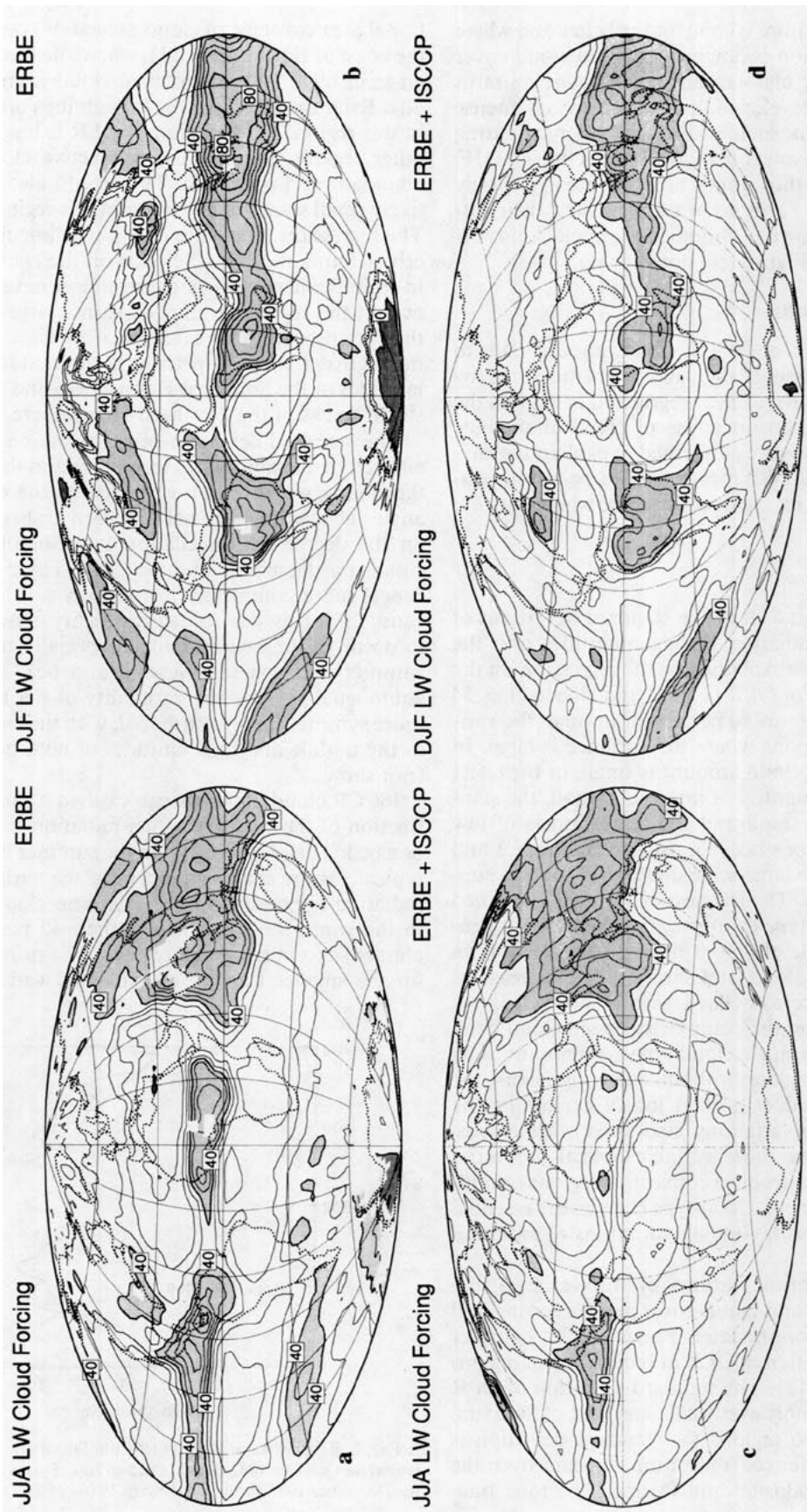

FIG. 9. Forcing of the net radiation balance through the longwave effect of clouds, as inferred from the regression on ISCCP data and the ERBE clear-sky scene identification for JJA and DJF seasons. Contour interval is 10 W m^{-2}. Values greater than 40 W m^{-2} are shaded and values less than zero are heavily shaded.

radiation is the cancellation between the solar and longwave effects of clouds on the net radiation. A correlation often exists between the albedo of a cloud and its cloud-top altitude, so that as the shortwave effect of a cloud gets larger, its longwave effect also increases to partly compensate. This causes the variance of the net radiation to be reduced, which provides a smaller signal for the regression to capture. A particular value of the net radiation can be produced in many different ways by combining clouds with various albedo and top temperature pairings. Thus, the net radiation is less well defined by the amount and type of cloud than are the OLR or albedo individually. This point was also emphasized by Dhuria and Kyle (1991).

b. *Clear-sky fluxes and cloud forcing from linear regression*

One possible application of the multiple linear regression analysis is to investigate the role of clouds in modifying the energy balance of the earth. The regression equations are of the form,

$$R = a_0 + \sum_{i=1}^{5} a_i C_i \qquad (1)$$

where R is, for example, the net radiation, C_i is the fractional coverage by cloud type i, and a_i are the coefficients of the regression. If the regression forms a good approximation of the effect of cloud on the radiation balance, then we may interpret the regression in the following way:

$$R = R_{\text{clear}} + \sum_{i=1}^{5} \Delta R_i C_i . \qquad (2)$$

Here R_{clear} is the net radiation in the absence of clouds and ΔR_i is the change in net radiation associated with 100 percent coverage by cloud type i. It may or may not be appropriate to interpret the regression equation in the manner indicated by (2), depending on the nature of the data given to the regression. If the dataset from the 2.5° × 2.5° region in question actually contains within it a large range of variation of each cloud type present, and the relationship of the radiation balance to the cloudiness is approximately linear, then the regression coefficients can probably be safely interpreted as in (2). On the other hand, if the fractional area coverage by cloud is relatively constant, especially if it remains almost always overcast, then the regression receives no information on what the clear-sky radiances are. The regression will attempt to fit as closely as possible the variance around a nearly overcast sky, and the intercept of the regression may be a poor approximation to the clear-sky value. If the intercept is seriously in error, then interpreting the remaining coefficients as the sensitivity of the radiation balance to individual cloud types is questionable also.

It is of interest to compare the intercept of the regressions with the clear-sky values determined from the ERBE data products, where the scene identification algorithm is used to select a subset of the ERBE scanner pixels that are declared to be free of the effects of cloud (Ramanathan et al. 1989; Harrison et al. 1990). The clear-sky OLR estimated from the regressions is in reasonable agreement with those of the ERBE clear-sky climatology in most regions (Fig. 7). Interesting differences appear in the regions of intense tropical convection, however, where the regression gives much lower clear-sky OLR values than the ERBE climatology. The ERBE clear-sky climatology almost never goes as low as 270 W m^{-2} in these regions, whereas the regression provides estimates as low as 240 W m^{-2} in those regions of most intense and persistent convection. We also observe that in many cases the regression produces a slightly higher estimate of the clear-sky OLR

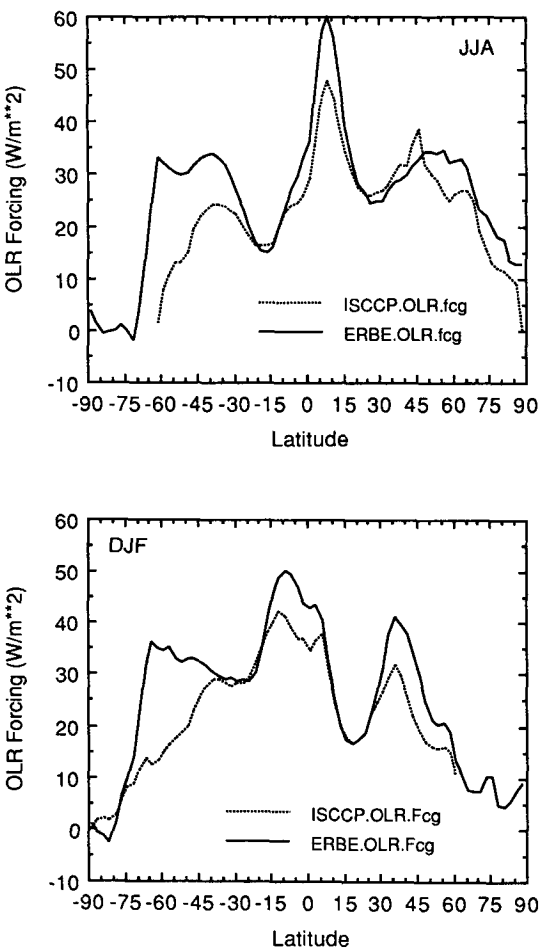

FIG. 10. Zonal averages of the longwave cloud forcing of net radiation for the (a) JJA and (b) DJF seasons derived from ERBE average and clear-sky climatologies (solid line) and from regression between ISCCP clouds and ERBE OLR (dotted line).

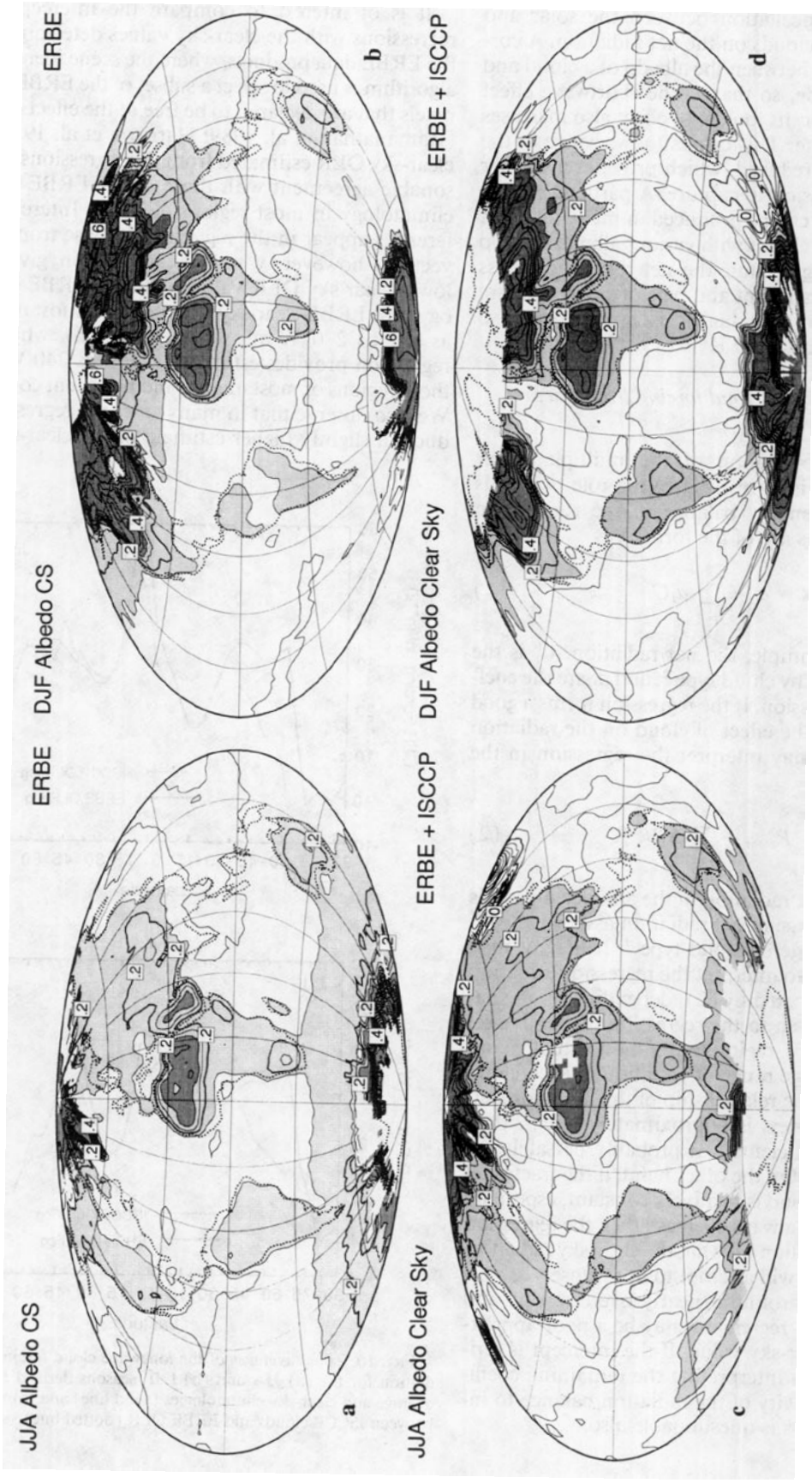

FIG. 11. As in Fig. 7 except for clear-sky albedo. Contour interval is 0.05. Values greater than 0.15 are shaded and values greater than 0.3 are heavily shaded.

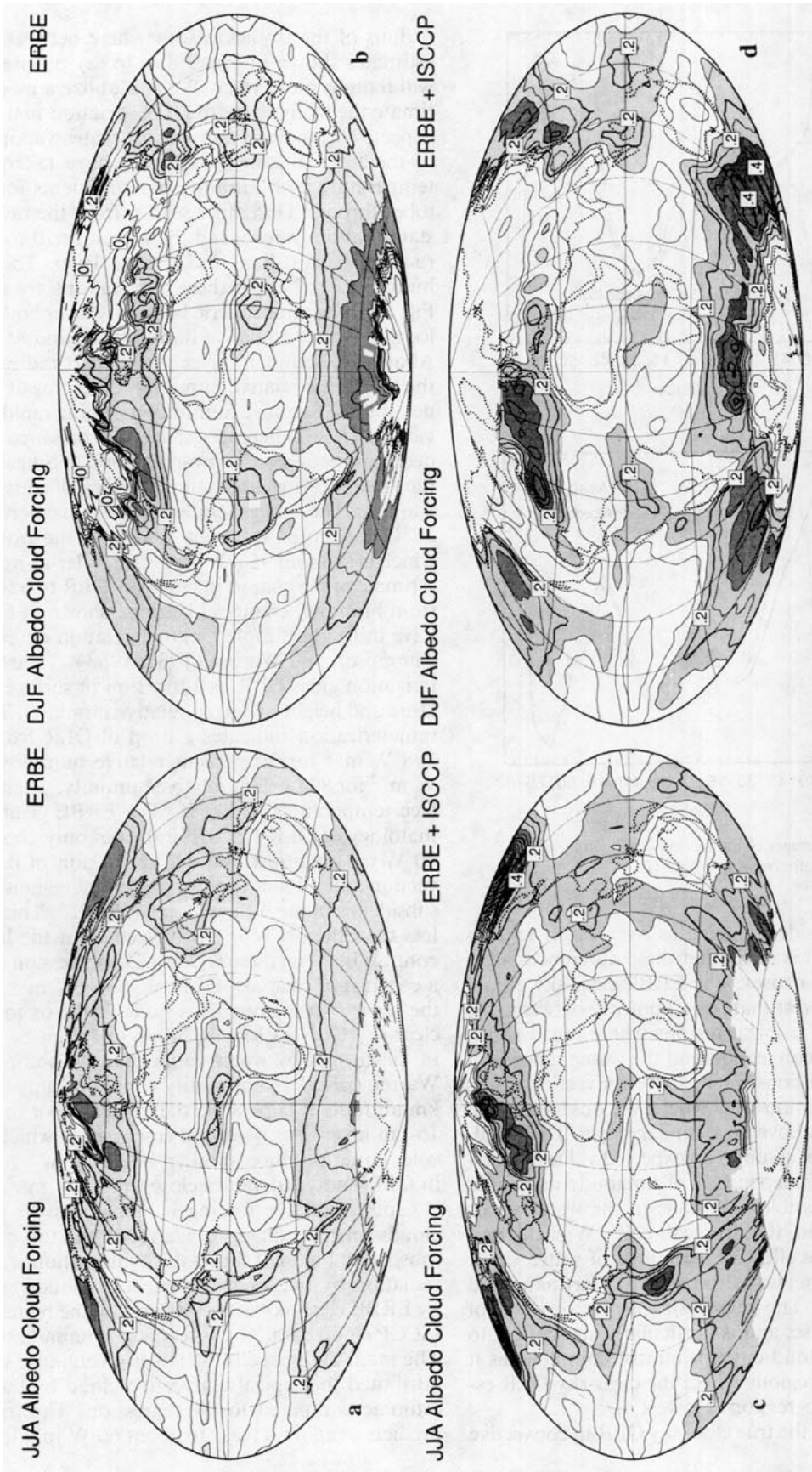

FIG. 12. Forcing of the albedo by clouds, estimated by the two methods described in the text. Contour interval is 0.05. Values greater than 0.15 are shaded and values greater than 0.3 are heavily shaded.

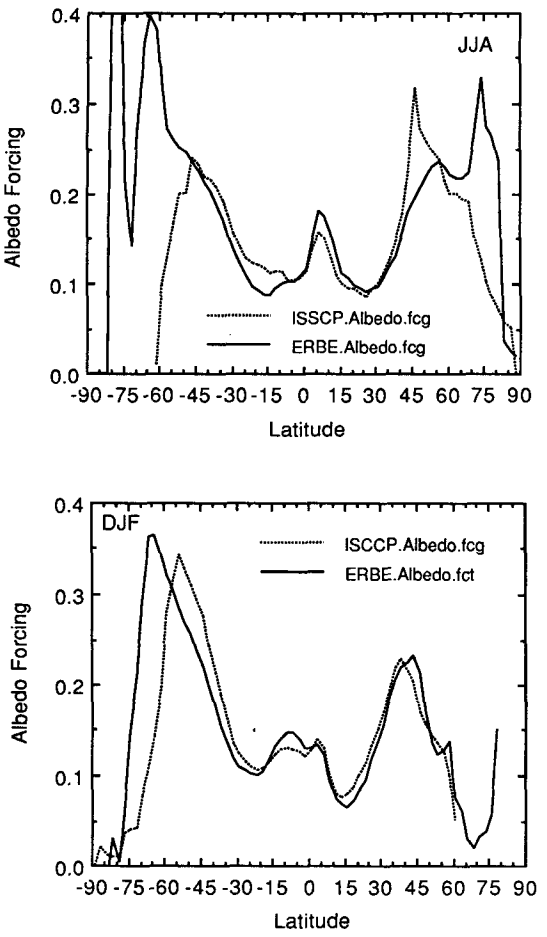

FIG. 13. Zonal averages of the forcing of albedo by clouds, otherwise as in Fig. 10.

in regions of subsidence, such as over desert regions during summer. It is likely that these differences are a result of multiple causes. The ERBE clear-sky climatology may underestimate the contrast between the clear-sky OLR of tropical regions where mean subsidence suppresses convection and the water vapor profile, and tropical regions where active convection drives mean upward motion and where we observe much more water vapor above the boundary layer. The ERBE scene identification assumes an expected value of clear-sky OLR that is independent of longitude and takes no account of possible variations in the water vapor distribution within the tropical belt (Wielicki and Green 1989). The effect of variations of water vapor on net cloud forcing was also noted by Hartmann and Doelling (1991). The regression has its own set of problems, of course, and is particularly susceptible to error where the cloud cover is almost complete, as it is in some of the regions where the clear-sky OLR estimate from the regression is lowest.

We suspect that the true clear-sky OLR in convective regions of the tropics is somewhere between the two estimates shown in Fig. 7, but to say precisely where will require more work. We can utilize a model to estimate the likely range of OLR variation that could be expected from variations in the water vapor content of the tropical atmosphere. We have taken average temperature and humidity measurements for the October through December season from the rawinsonde station at Singapore, and the December through February means at San Jose, Puerto Rico. The average humidity profiles for these two stations are shown in Fig. 8. In the atmospheric boundary layer both of these locations have a relative humidity around 85 percent. Above the boundary layer they depart radically, with the Singapore relative humidity remaining at high values and the San Jose humidity dropping rapidly to low values. These differences reflect the presence of active deep convection and upward motion at Singapore and the mean downward motion and lack of convection at San Jose. The surface temperature at Singapore is about 26°C and drops to about −80°C at the tropopause, which is at about 95 mb. To get an order-of-magnitude estimate of the change in clear-sky OLR to be expected from humidity changes like those shown in Fig. 8, we have utilized a simple parameterization developed by Thompson and Warren (1982, 1983). Their parameterization gives OLR as a function of surface temperature and height-averaged relative humidity. Their parameterization indicates a drop of OLR from about 298 W m^{-2} for 20 percent relative humidity to 263 W m^{-2} for 80 percent relative humidity, when the surface temperature is 300 K. The ERBE clear-sky climatology of OLR for DJF indicates only about a 15–20 W m^{-2} contrast between the region of deep convection around Singapore and adjacent regions of mean subsidence in the Indian Ocean (Fig. 7b). This is much less than the 35 W m^{-2} expected from the humidity contrast between these regions. The regression indicates a contrast in clear-sky OLR of 35–40 W m^{-2} between the same two regions. It is difficult for us to say if a clear-sky OLR as low as 240 W m^{-2} can be induced in the tropics by water vapor alone. Thompson and Warren considered humidity variations only up to 12-km altitude. It is possible that water vapor in the 12–16-km layer of the tropical tropopause, which is very cold, could produce another 10–20 W m^{-2} reduction in OLR and yield values close to 240 W m^{-2}.

Cloud radiative forcing is defined as the effect of clouds on the radiation balance at the top of the atmosphere. Figure 9 shows the contributions to the net radiation by the longwave effect of clouds estimated by ERBE clear-sky estimates and by the regression on ISCCP cloud data. The agreement is remarkably good. The main difference is the larger greenhouse warming attributed to tropical convective cloud by the ERBE estimate compared to the regression. The regression predicts a rapid increase to about 60 W m^{-2} longwave

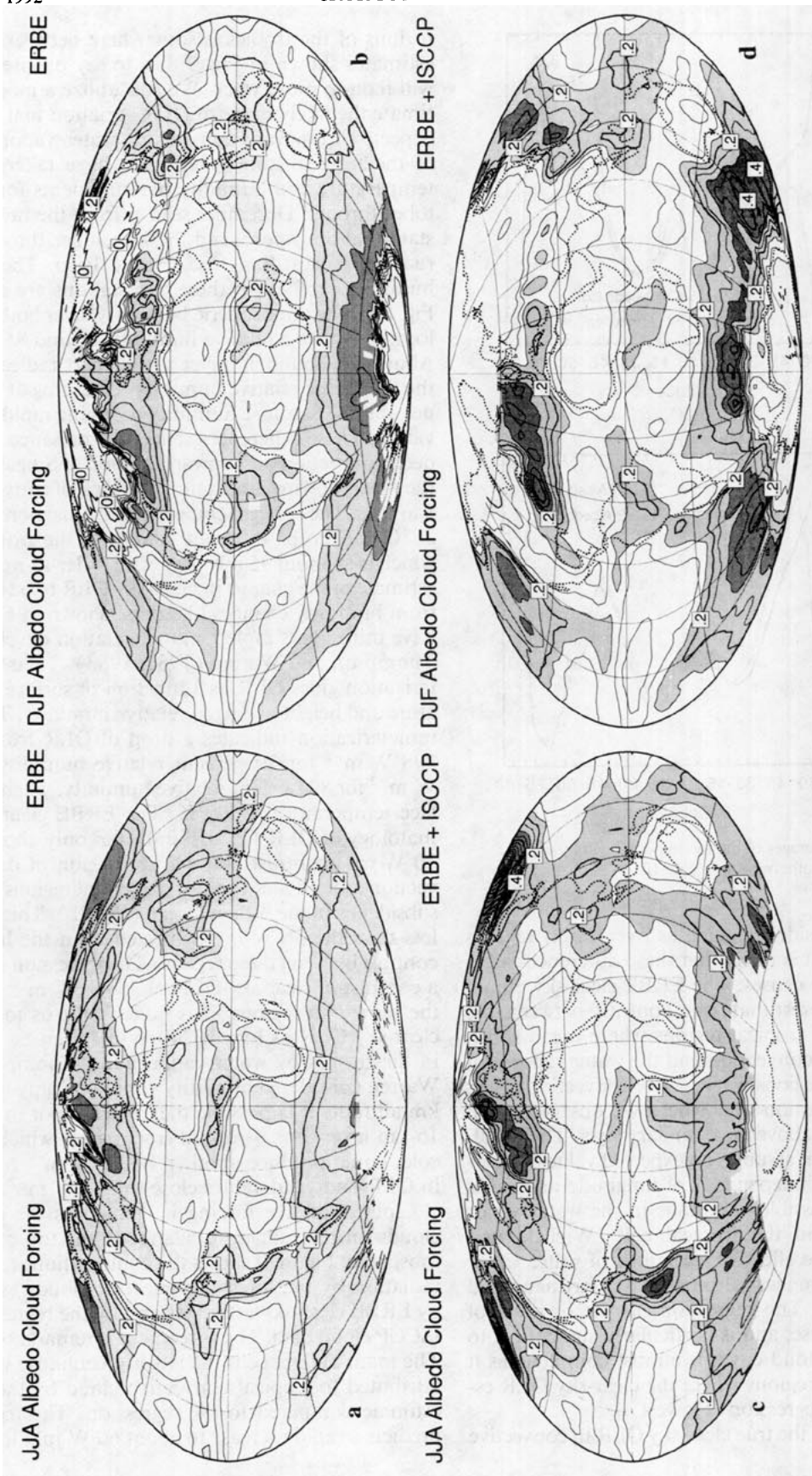

FIG. 14. As in Fig. 7 except for clear-sky net radiation. Contour interval is 20 W m^{-2}. Values greater than 80 W m^{-2} are shaded and values less than zero are heavily shaded.

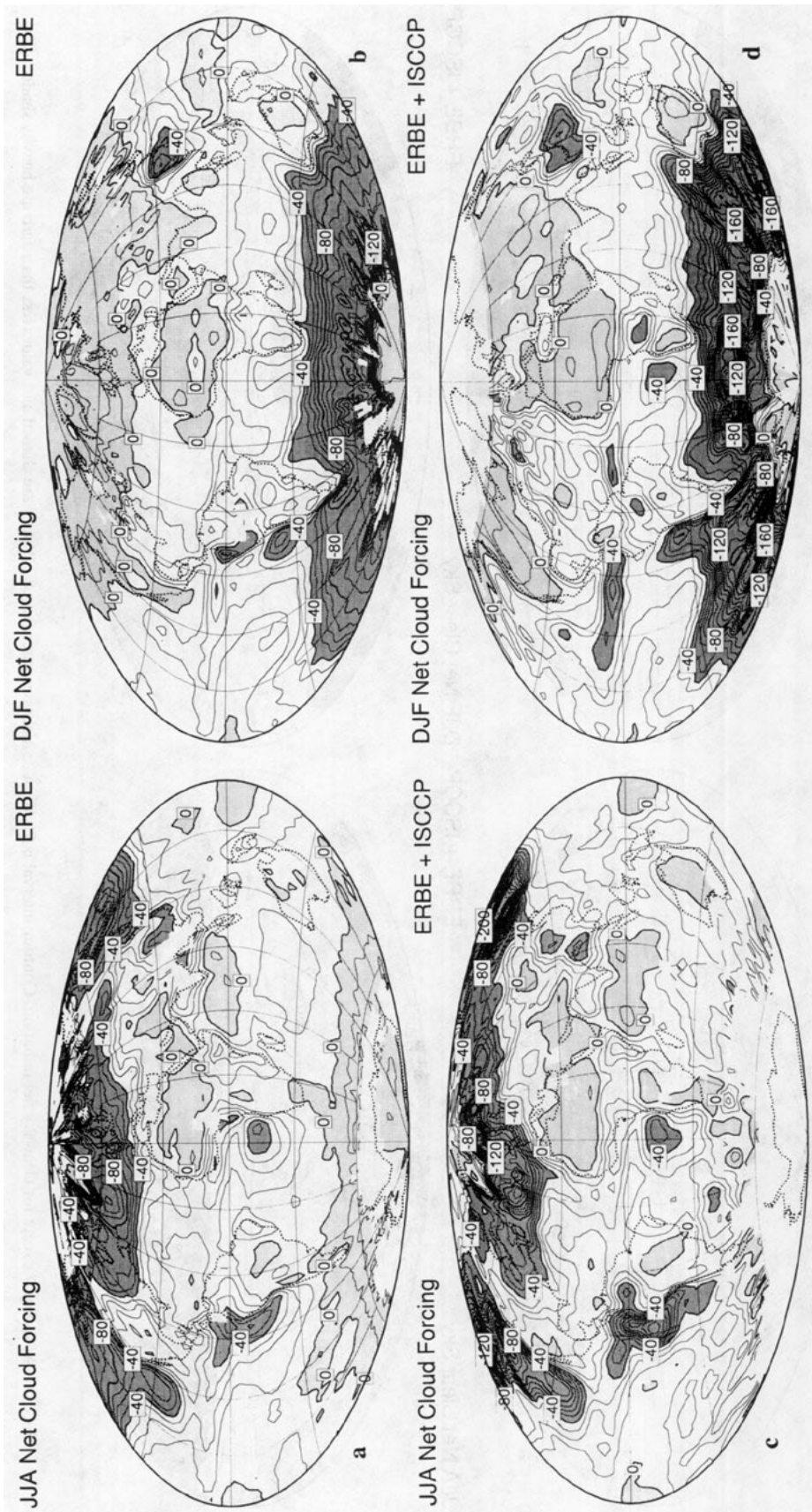

FIG. 15. As in Fig. 9 except forcing of the net radiation balance by clouds. Contour interval is 20 W m^{-2}. Values greater than zero are shaded and values more negative than −40 W m^{-2} are heavily shaded.

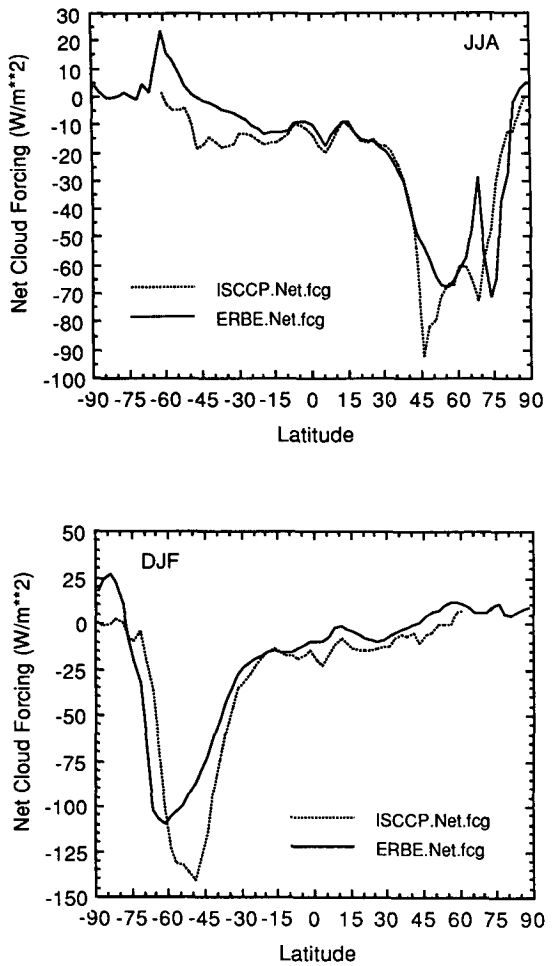

FIG. 16. Zonal averages of the forcing of net radiation by clouds, otherwise as in Fig. 10.

trapping across the edge of the high-cloud region and relatively flat values within it. The ERBE longwave cloud forcing also increases rapidly across the edge of the convective region, but then continues to increase within it and peaks at values in excess of 80 W m^{-2} in the regions of most intense convection.

A simpler view of the difference between the longwave cloud forcing estimates can be obtained by plotting their zonal averages (Fig. 10). The zonal averages agree almost exactly in the subtropical dry belts, but depart significantly in the humid tropics and in midlatitudes, where the regression estimates show a smaller longwave forcing than the ERBE estimates. The difference is greatest near 60°S, where the ERBE estimate of longwave cloud forcing is near 30 W m^{-2} and the regression estimate is only 10 W m^{-2}. The ISCCP data indicate nearly 90 percent cloud cover along 45°–60°S in all seasons, so that the clear-sky fluxes are difficult to measure in this region.

The clear-sky albedos from the regression are also in overall agreement with the ERBE estimates, but some regions where the regression fails are evident (Fig. 11). Over the North Pacific Ocean during JJA the regression indicates large negative clear-sky albedos—an absurd result. Over the stratus cloud region west of South America during JJA and over the southern Indian Ocean during DJF the regression also gives negative albedos. These serious problems with the interpretation of the regression intercept as the clear-sky value probably result from the fact that in these regions substantially clear skies covering a 2.5° region are almost never observed, so that the dataset does not contain the information necessary to constrain the intercept to a physically reasonable value. The day-to-day fluctuations of albedo and the cloud differ little from the values for almost overcast skies, and in such regions the extrapolation of the resulting regression equation to zero cloudiness can result in nonsense.

The regression method appears to produce a reasonable estimate of the clear-sky albedo over the sea ice around Antarctica. The ERBE scene identification algorithm is not given information on the position of the sea ice around Antarctica, and assumes open ocean right up to the edge of the continent. For this reason ERBE estimates of clear-sky values around Antarctica are usually missing, since the albedos are never low enough to qualify as clear ocean. The regression method indicates an increase in the clear-sky albedo at about the expected position of the ice edge in each season. During winter the ice edge extends equatorward of 60°S in the Atlantic Ocean and the regression shows high clear-sky albedos there. The regression also shows the high clear-sky albedos associated with the sea ice in the Weddell Sea, downwind of the Palmer Peninsula, during DJF.

The change of albedo associated with the presence of cloud cover is shown in Fig. 12. The regression estimates cannot be trusted in the regions where the clear-sky values were shown to be seriously in error. During DJF the regression estimate shows the cloud forcing of albedo to maximize at about 50°S and decrease over the sea ice surrounding Antarctica. Zonal averages of the albedo cloud forcing estimates are in good agreement in the tropics, but differ significantly in high latitudes, especially during JJA (Fig. 13). The main disagreement during DJF is over the Southern Hemisphere, where in midlatitudes the regression estimate first exceeds the ERBE values in midlatitudes and then decreases rapidly at the edge of the sea ice, while the ERBE estimates continue to increase right up to the edge of the continent of Antarctica.

The regression estimate of clear-sky net radiation also shows more variability over the oceans than is expected (Fig. 14). This is partly a problem with the regression procedure and partly because we have used only one season of data to perform the regressions.

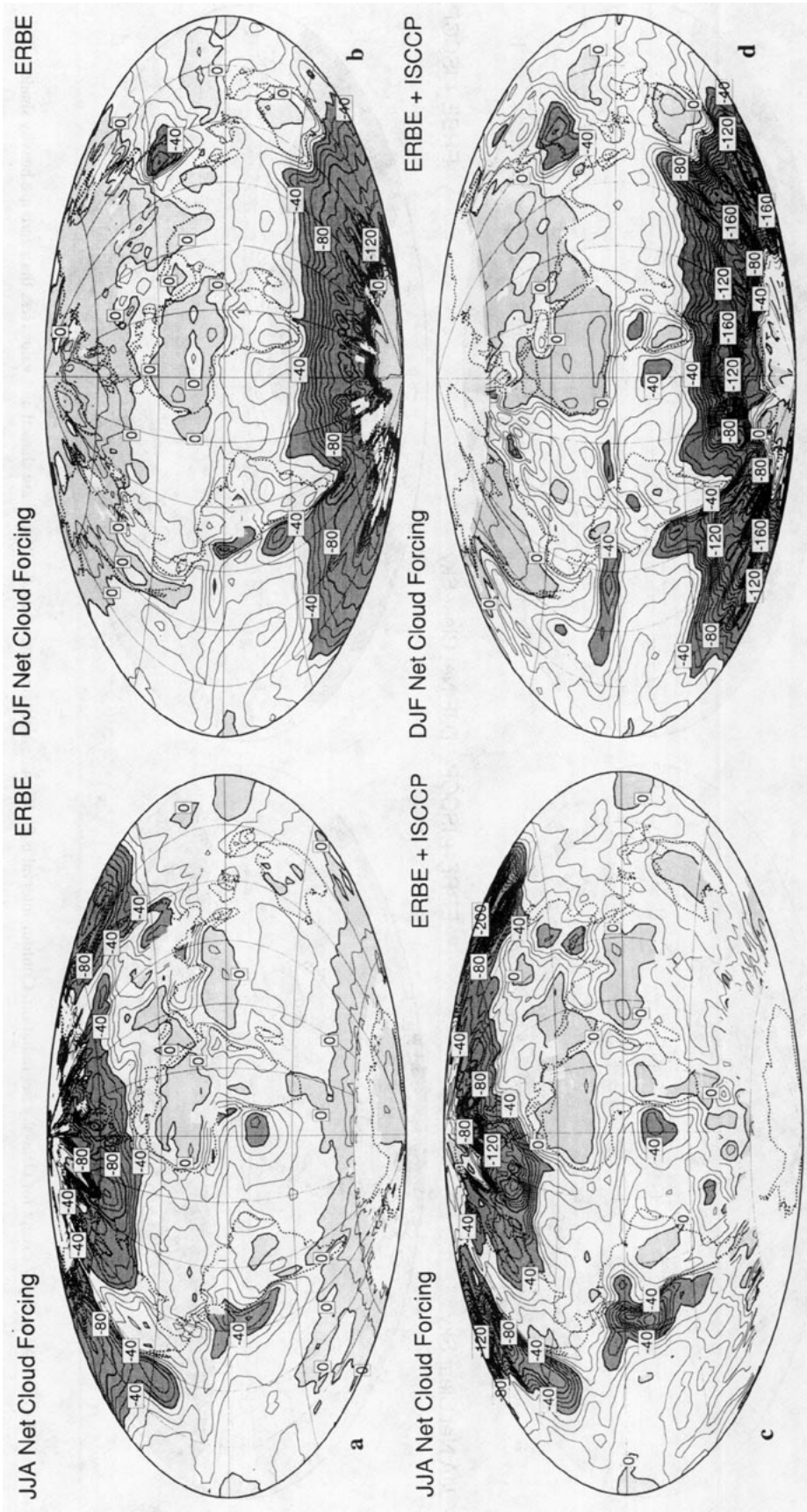

FIG. 17. Longwave cloud forcing of net radiation by cloud type 1 (high-thin) and cloud type 2 (high-thick). Contour interval is 5 W m^{-2}. Values greater than 15 W m^{-2} are shaded and values greater than 40 W m^{-2} are heavily shaded.

The cloud forcing of net radiation determined by ERBE and by the current regression method are in remarkable agreement considering the small fraction of variance explained by the regression (Fig. 15). In the tropics the two methods produce very nearly the same estimate for zonal-average cloud forcing of net radiation (Fig. 16). The main discrepancies occur in high latitudes of the summer hemisphere over oceans, where the regression method indicates larger net cooling by clouds than the ERBE estimates. The differences are consistent with those inferred from the albedo comparisons, and the largest discrepancies occur in those regions where the regression inferred negative clear-sky albedos. The largest discrepancies again appear over the southern oceans during DJF.

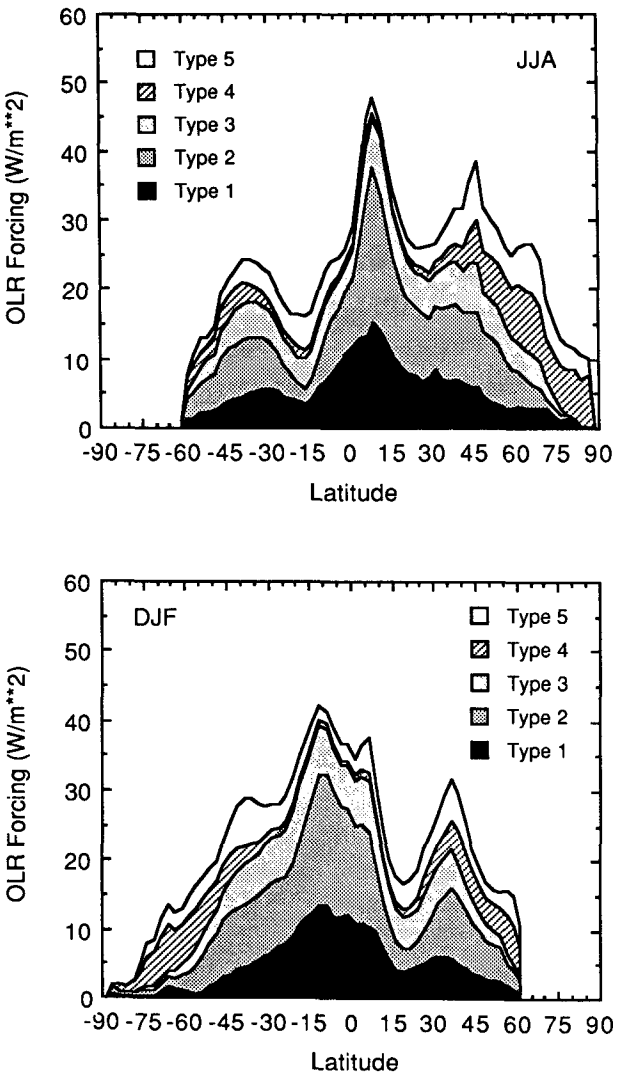

FIG. 18. Area diagram of contributions by individual cloud types to the total zonal average longwave effect of clouds on net radiation. Shaded areas indicate contributions by each cloud type to the total cloud forcing. Areas are shown cumulatively, so that the top curve represents the latitudinal distribution of total longwave cloud forcing.

c. *Radiative forcing by individual cloud types*

The comparison of the current regression method with the ERBE clear-sky climatology shows sufficient agreement that we can attempt to use the regression to show the contributions to cloud forcing by individual cloud types, at least in the tropics. It must be remembered that these estimates are based upon stepwise regressions of daily variations of radiation budget quantities on daily estimates of cloud amounts. It is an assumption that these regressions are indicative of the contributions of particular cloud types to the climatological radiation balance. The forcing estimate is the product of the sensitivity of the radiation quantity to the particular cloud type, which is the coefficient a_i of the regression equation (1), and the amount of the cloud type in the region, C_i.

As would be expected, the highest clouds contribute most to the longwave cloud forcing in tropical regions (Fig. 17). Nearly equal contributions are made by the thick and thin varieties of high cloud, since they have approximately the same cloud-top pressure and are present in approximately the same abundances. In middle and high latitudes, significant contributions to the zonal-average longwave cloud forcing are contributed by middle and low clouds (Fig. 18). The smaller sensitivity of the OLR to these clouds is offset by their greater abundance in midlatitudes.

Forcing of the albedo is contributed primarily by clouds with larger optical depths—types 2 and 4—and by abundant low clouds. High thick clouds dominate the albedo forcing in convective regions of the tropics and in midlatitude storm tracks (Fig. 19). Albedo forcing by low clouds is very important in the stratus cloud regions and in high latitudes, especially in the summer hemisphere. Middle thick clouds provide significant albedo forcing in middle and high latitudes (Fig. 20). The optically thin clouds of types 1 and 3 contribute only weakly to the forcing of albedo, according to the regression.

The largest contributions to net cloud forcing are provided by low clouds, especially in the tropical stratus cloud regions and the summer hemisphere (Fig. 21). Low clouds are abundant, and act to reduce the radiation balance by reflecting solar radiation. High thick clouds also provide significant reductions to the radiation balance, since they reflect more solar radiation than they trap longwave emission. High- and middle-level clouds with relatively low optical depths do not enter very strongly into the regression equations for net radiation. High thin clouds make a small positive contribution to the net radiation in tropical latitudes—amounting to about 5 W m^{-2} in the zonal average (Fig. 22).

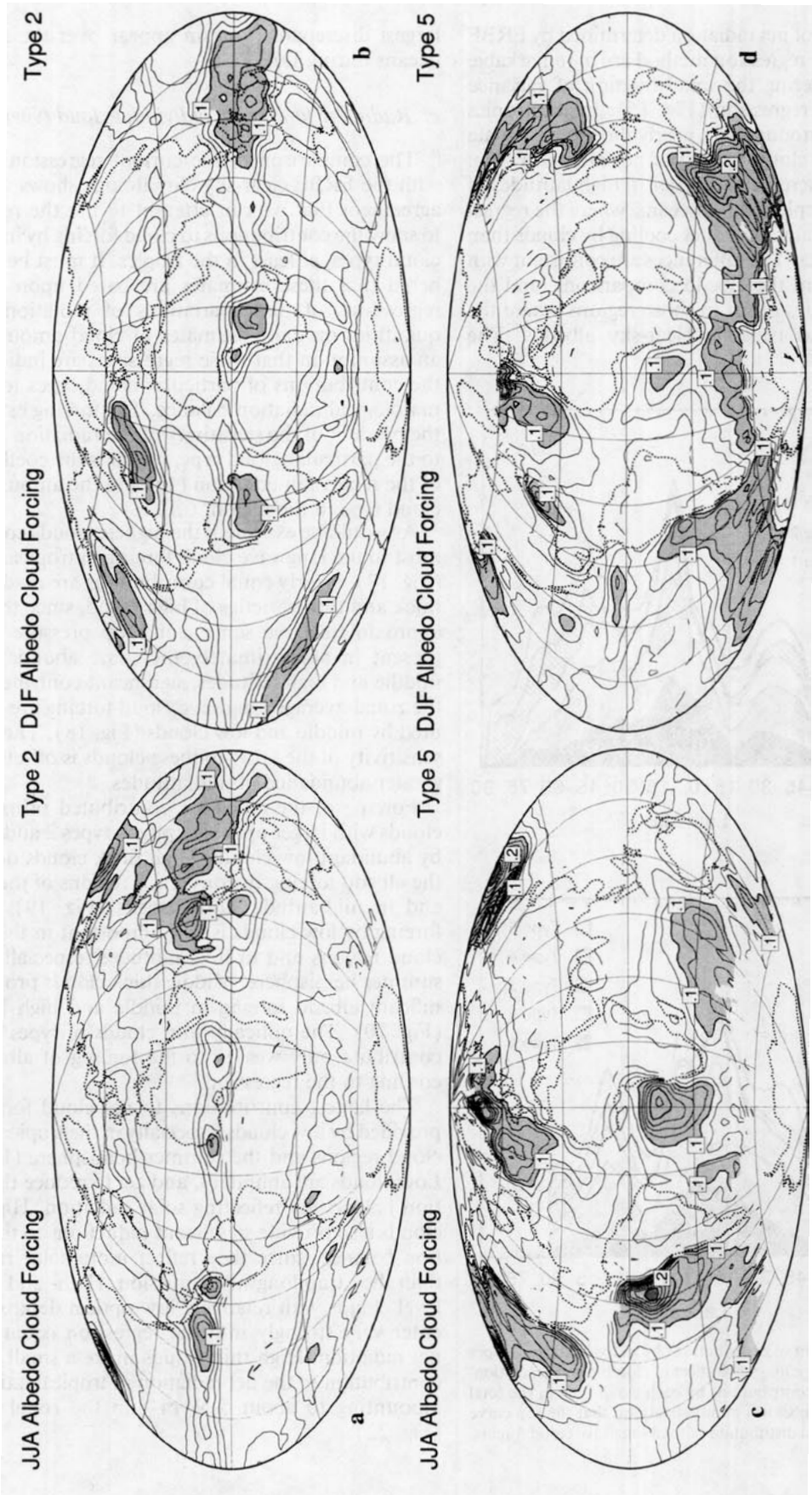

FIG. 19. Albedo forcing by cloud types 2 (high-thick) and 5 (low). Contour interval is 0.025. Values greater than 0.1 are shaded and values greater than 0.3 are heavily shaded.

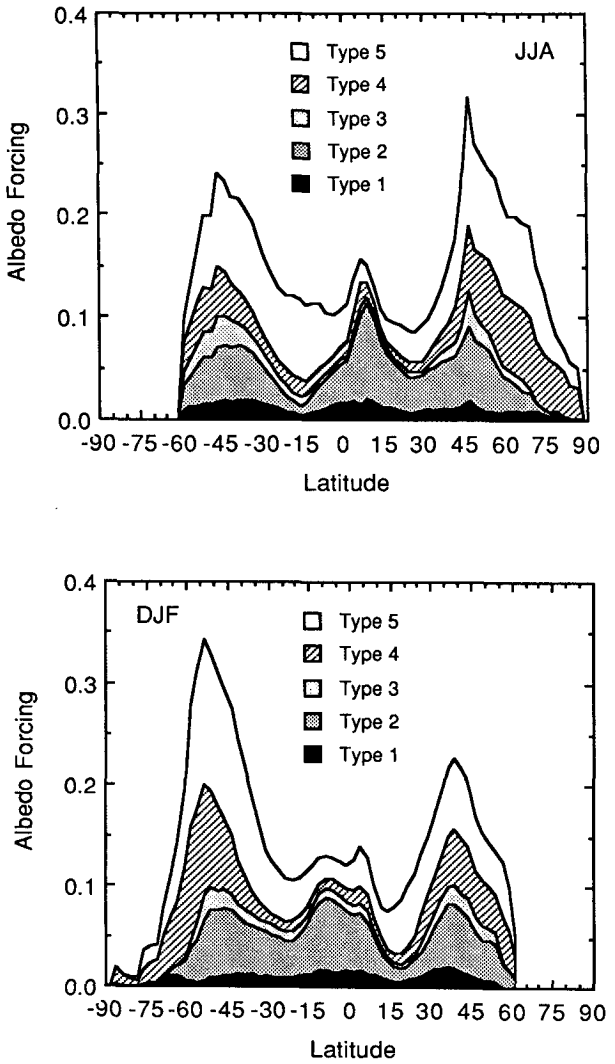

FIG. 20. Area diagram of zonal average cloud forcing of albedo by cloud type.

Cloud forcing by type, averaged over the area of the globe where we have cloud data, is shown in Table 1. These are very close to what would be obtained from global data, since the cloud forcing in the polar darkness is small and the areal extent of polar darkness is a small fraction of the global surface area. High clouds contribute the most to the cloud reduction of OLR, but significant contributions also come from middle and low clouds. The total longwave forcing of about 26 W m^{-2} is about 5 W m^{-2} smaller than ERBE estimates of 31 W m^{-2} (Harrison et al. 1990). The albedo forcing is about equal to the ERBE estimate of 15 percent, and is contributed by the optically thick clouds. This agreement is deceptive, however, since the result in Table 1 is a simple area average, and an insolation-weighted average might not agree quite so well with the ERBE estimate, which is properly insolation weighted.

High, thick clouds contribute almost as much to the albedo forcing as low clouds, despite their smaller fractional area coverage and the fact that the albedo forcing by low clouds is known to be significantly overestimated in some regions. The very powerful albedo forcing of high, thick clouds is offset by the large OLR forcing of these clouds, so that their contribution to net cloud forcing is only a little more than a third of that for low clouds. Low clouds comprise about 40% of the total cloud cover and appear to contribute about 60% of the net cloud forcing. The net radiative cloud forcing estimated by regression of ISCCP cloud amounts, about -27 W m^{-2}, is more strongly negative than that of the ERBE estimates, which put the net cloud forcing at about -17 W m^{-2} (Harrison et al. 1990). The difference of the regression estimate from the ERBE estimates comes in about equal parts from the smaller estimate of the reduction in longwave emission caused by clouds and from the larger albedo enhancement over the midlatitude oceans in summer. The uncertainty of the ERBE estimates is believed to be about 5 W m^{-2}, so the current estimate of -27 W m^{-2} is significantly different. If each estimate is given an uncertainty of 5 W m^{-2}, a consensus value of -22 W m^{-2} could be consistent with both.

The sensitivity of the radiation budget quantities to the amount of a particular type of cloud can be estimated by dividing the net forcing from a particular cloud type by the fraction of that type of cloud present. Use of the numbers in Table 1 reveals that the net radiation is actually more sensitive to high, thick clouds of type 2 than it is to low clouds. If we average the estimates for JJA and DJF, the sensitivity to type-2 clouds is -80 W m^{-2} per unit of area coverage, and the sensitivity to type-5 clouds is -63 W m^{-2}.

4. Conclusions

Linear stepwise regression has been used to express ERBE radiation budget quantities in terms of five generic cloud types defined by ISCCP C-1 cloud amount estimates. Cloud-type information is important in such regressions. The five-type description of cloudiness explains about twice as much variance as a regression on total cloud cover alone for OLR and albedo, and more than twice as much for net radiation. The five-type cloud description explains about 80 percent of the variance of OLR and albedo in most regions, but only about 40 percent of net radiation. Because of frequent compensation between the OLR and albedo effects of clouds, the net radiation is less uniquely related to the cloud distribution than either OLR or albedo. The relationship of net radiation to cloudiness is multiple valued, since the same net radiation can be produced by a wide variety of possible cloud configurations.

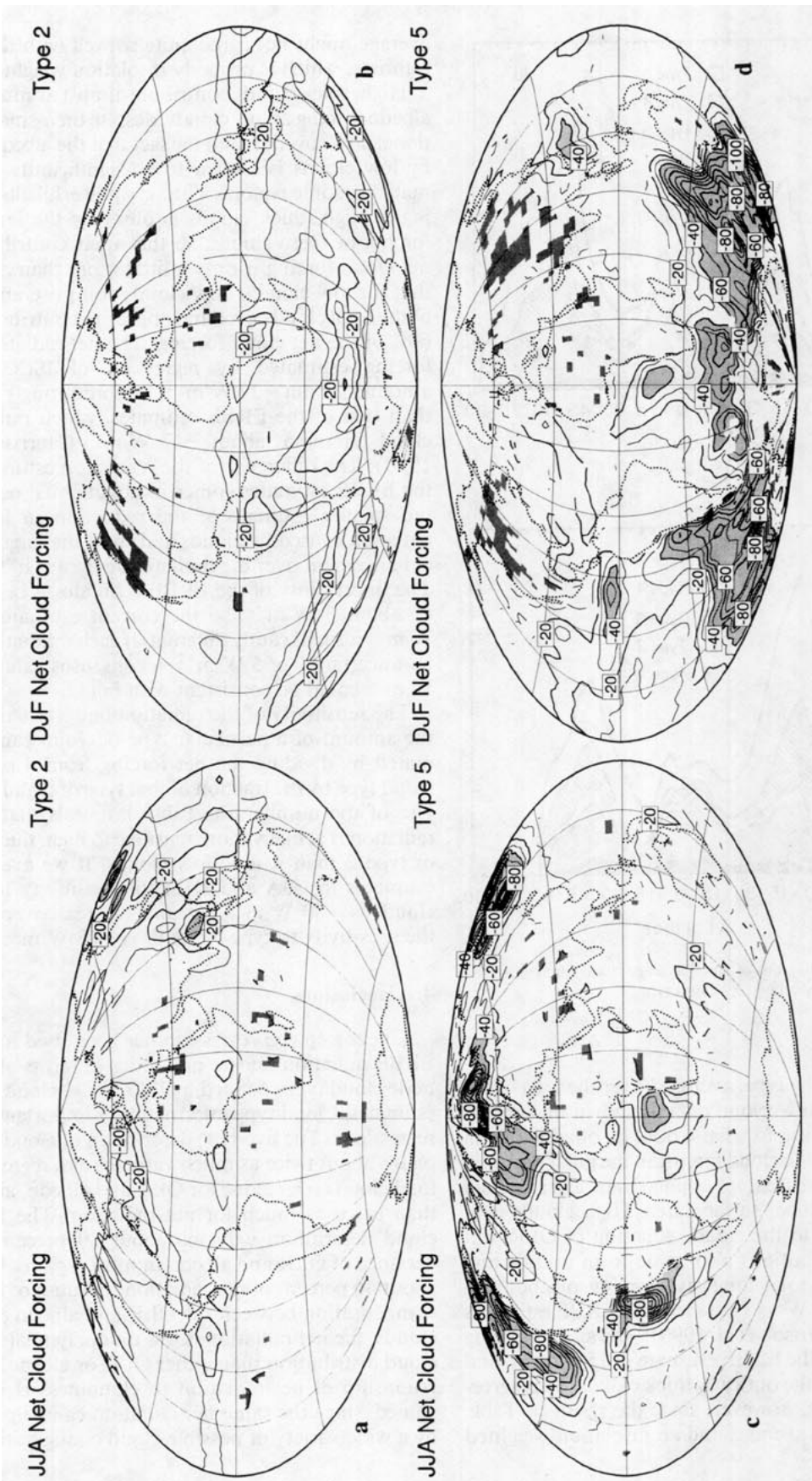

FIG. 21. Forcing of net radiation by cloud types 2 (high-thick) and 5 (low). Contour interval is 10 W m^{-2}. Values more negative than -40 W m^{-2} are shaded and values greater than zero are heavily shaded.

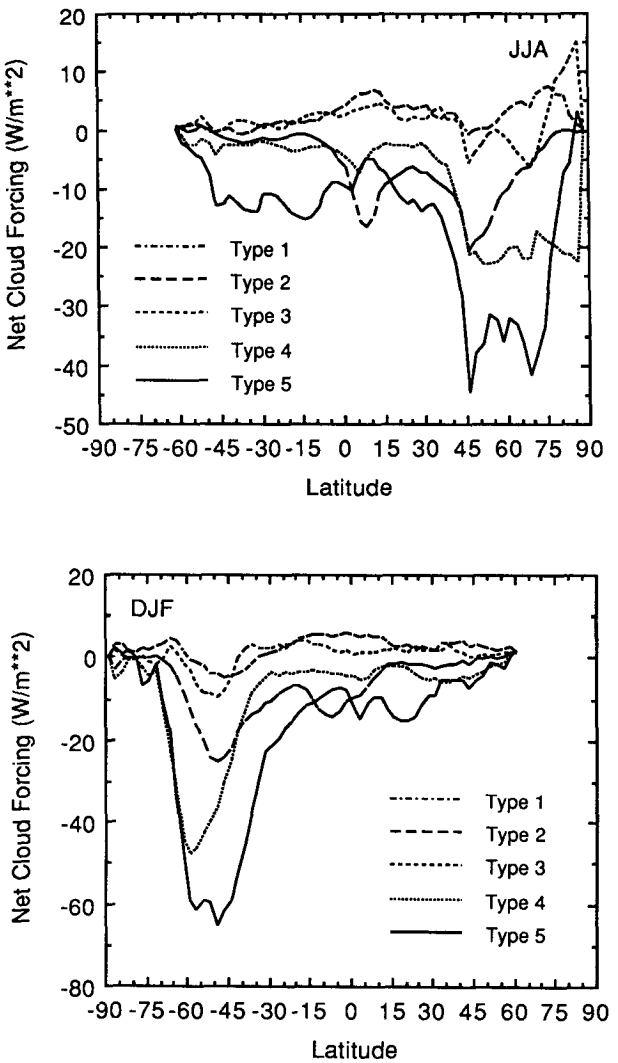

FIG. 22. Zonal average forcing of net radiation by individual cloud types.

The regression analysis produces clear-sky estimates and total cloud forcing estimates in good agreement with those derived from ERBE clear-sky and average composites, except in those regions where the clouds are so persistent that clear scenes are rarely observed. In such regions regression can produce unrealistic estimates of cloud forcing, even when the regression explains a substantial fraction of the variance. Regions of very persistent cloudiness occur over the oceans in high latitudes, in the regions of most intense convection in the tropics, and in some subtropical stratus regions. Since regression can fail catastrophically, care must be exercised in interpreting the results of regression analyses of the type described here.

Comparison of the ERBE clear-sky climatology, the regression results, and model calculations of clear-sky fluxes suggests that the ERBE clear-sky climatology overestimates the clear-sky OLR in tropical regions where deep convection moistens the troposphere with large amounts of water vapor. For this reason the ERBE estimates of longwave cloud forcing in these regions may be too large by as much as 20 W m^{-2}. This discrepancy is associated with the difficulty of separating the longwave effect of cloud liquid water and ice from the longwave effect of the enhancement of upper-tropospheric water vapor that normally accompanies deep convection in the tropics.

Regression of ERBE data on ISCCP cloud types provides an estimate of the contributions of individual cloud types to the net cloud forcing of the earth's energy balance. Clouds with visible optical depths less than about 9 are defined here as thin, and those with greater optical depths are defined as thick. The results presented here indicate that low clouds provide the largest net cloud forcing—about -16 W m^{-2} or 60% of the total net cloud forcing. High- and midlevel optically thick clouds each make contributions of about -7 W m^{-2} to the net radiation. High, thick clouds make a larger contribution to net cooling per unit area than low clouds. High- and midlevel optically thin clouds make small positive contributions to global net cloud forcing, because of a near compensation between their effects on OLR and absorbed solar radiation.

It is hoped that these preliminary estimates will be useful in validating predictions of cloud radiative effects in climate models. We believe it will be important to verify that the contributions to net cloud radiative

TABLE 1. Global area-averaged cloud forcing by type of cloud. OLR and net radiation are given in W m^{-2} and albedo and cloud fractional coverage are given in percent. The last column is the sum over all cloud types and the average of the JJA and DJF season. The regions poleward of about 60° in the winter hemisphere are not included in the area average.

	Type 1 High, thin		Type 2 High, thick		Type 3 Mid, thin		Type 4 Mid, thick		Type 5 Low		Sum Average
	JJA	DJF	JJA	DJF	JJA	DJF	JJA	DJF	JJA	DJF	
C_i	10.2	10.0	8.5	8.8	10.7	10.7	6.5	8.2	27.2	25.9	63.3
OLR	6.5	6.3	8.4	8.8	4.8	4.9	2.4	2.4	3.5	3.5	25.8
Albedo	1.2	1.1	4.1	4.2	1.1	1.0	2.7	3.0	5.8	5.6	14.9
Net	2.4	2.3	−6.4	−7.5	1.4	0.8	−6.6	−8.5	−15.1	−18.2	−27.6

forcing by individual cloud types is as observed, as well as to verify that the total cloud forcing is realistic.

Acknowledgments. This research was supported by NASA under the Earth Radiation Budget Experiment, Contract NAS1-18157 through Langley Research Center. We benefited from conversations with C. B. Leovy and S. G. Warren. P. H. Stone provided useful suggestions to improve the manuscript. G. C. Gudmundson provided editorial assistance.

REFERENCES

Abbot, C. G., and E. E. J. Fowle, 1908: Annals of the Astrophysical Observatory of the Smithsonian Institution, **2,** Smithsonian Institution, Washington, D.C.

Barkstrom, B. R., and G. L. Smith, 1986: The Earth Radiation Budget Experiment (ERBE). *Bull. Amer. Meteor. Soc.,* **65,** 1170–1185.

Cess, R. D., 1976: Climate change: An appraisal of atmospheric feedback mechanisms employing zonal climatology. *J. Atmos. Sci.,* **33,** 1831–1843.

Dhuria, H. L., and H. L. Kyle, 1991: Cloud types and the tropical earth radiation budget. *J. Climate,* **3,** 1409–1434.

Hansen, J., A. Lacis, D. Rind, G. Russell, P. Stone, I. Fung, R. Ruedy, and J. Lerner, 1984: Climate sensitivity: Analysis of feedback mechanisms. *Climate Processes and Climate Sensitivity. Geophys. Monogr.,* **29** (*Maurice Ewing* **5**), 130–163.

Harrison, E. F., P. Minnis, B. R. Barkstrom, V. Ramanathan, R. D. Cess, and G. G. Gibson, 1990: Seasonal variation of cloud radiative forcing derived from the Earth Radiation Budget Experiment. *J. Geophys. Res.,* **95**(D22), 18 687–18 703.

Hartmann, D. L., and D. A. Doelling, 1991: On the net radiative effectiveness of clouds. *J. Geophys. Res.,* **96,** 869–891.

——, V. Ramanathan, A. Berrior, and G. E. Hunt, 1986: Earth radiation budget data and climate research. *Rev. Geophys. Space Phys.,* **24,** 439–468.

Haurwitz, B., 1948: Insolation in relation to cloud type. *J. Meteor.,* **5,** 110–113.

Ockert-Bell, M. E., and D. L. Hartmann, 1992: The effect of cloud type on earth's energy balance: Results for selected regions. *J. Climate,* **5,** 1157–1171.

Ramanathan, V., R. D. Cess, E. F. Harrison, P. Minnis, B. R. Barkstrom, E. Ahmad, and D. L. Hartmann, 1989: Cloud-radiative forcing and climate: Results from the Earth Radiation Budget Experiment. *Science,* **243,** 57–63.

Rossow, W. B., and R. A. Schiffer, 1991: ISCCP cloud data products. *Bull. Amer. Meteor. Soc.,* **72,** 2–20.

Schneider, S. H., 1972: Cloudiness as a global climate feedback mechanism: The effects on the radiation balance and surface temperature of variations in cloudiness. *J. Atmos. Sci.,* **29,** 1413–1422.

Thompson, S. L., and S. G. Warren, 1982: Parameterization of outgoing infrared radiation derived from detailed radiative calculations. *J. Atmos. Sci.,* **39,** 2667–2680.

——, and ——, 1983: Parameterization of outgoing infrared radiation derived from detailed radiative calculations—Addendum. *J. Atmos. Sci.,* **40,** 1859.

Wetherald, R. T., and S. Manabe, 1980: Cloud cover and climate sensitivity. *J. Atmos. Sci.,* **37,** 1485–1510.

Wielicki, B. A., and R. N. Green, 1989: Cloud identification for ERBE radiative flux retrieval. *J. Appl. Meteor.,* **28,** 1133–1145.